Published online 12 March 2013 *Nucleic Acids Research, 2013, Vol. 41, No. 8* ***4709–4723***
doi:10.1093/nar/gkt160

Gradual processing of the ITS1 from the nucleolus to the cytoplasm during synthesis of the human 18S rRNA

Milena Preti[1,2], Marie-Françoise O'Donohue[1,2], Nathalie Montel-Lehry[1,2], Marie-Line Bortolin-Cavaillé[1,2], Valérie Choesmel[1,2] and Pierre-Emmanuel Gleizes[1,2,*]

[1]Laboratoire de Biologie Moléculaire Eucaryote, Université de Toulouse, UPS, F-31000 Toulouse, France and [2]CNRS, UMR 5099, F-31000 Toulouse, France

Received June 18, 2012; Revised February 14, 2013; Accepted February 19, 2013

ABSTRACT

Defects in ribosome biogenesis trigger stress response pathways, which perturb cell proliferation and differentiation in several genetic diseases. In Diamond–Blackfan anemia (DBA), a congenital erythroblastopenia, mutations in ribosomal protein genes often interfere with the processing of the internal transcribed spacer 1 (ITS1), the mechanism of which remains elusive in human cells. Using loss-of-function experiments and extensive RNA analysis, we have defined the precise position of the endonucleolytic cleavage E in the ITS1, which generates the 18S-E intermediate, the last precursor to the 18S rRNA. Unexpectedly, this cleavage is followed by 3′–5′ exonucleolytic trimming of the 18S-E precursor during nuclear export of the pre-40S particle, which sets a new mechanism for 18S rRNA formation clearly different from that established in yeast. In addition, cleavage at site E is also followed by 5′–3′ exonucleolytic trimming of the ITS1 by exonuclease XRN2. Perturbation of this step on knockdown of the large subunit ribosomal protein RPL26, which was recently associated to DBA, reveals the putative role of a highly conserved *cis*-acting sequence in ITS1 processing. These data cast new light on the original mechanism of ITS1 elimination in human cells and provide a mechanistic framework to further study the interplay of DBA-linked ribosomal proteins in this process.

INTRODUCTION

Ribosome production is a major metabolic activity, which is tightly regulated during cell cycle progression. It is now well established that defects in ribosome biogenesis can trigger stress response pathways that modulate cell cycle checkpoints, like activation of the tumor suppressor p53 by HDM2 or ARF (1–3). In Diamond–Blackfan anemia (DBA), a rare congenital erythroblastopenia, heterozygous mutations of ribosomal protein genes (10 identified to date) result in haploinsufficiency of the corresponding protein and defects in pre-ribosomal RNA (pre-rRNA) processing (4,5). This ribosomal stress can result in higher levels of p53, which appear to be fatal for erythroid progenitor differentiation (6), but it is likely that several stress response pathways are activated (2). Other rare genetic diseases, like the Shwachman–Diamond syndrome or the Treacher Collins syndrome, are also linked to defects in ribosome synthesis (7,8). This has led to the definition of a new class of pathologies named ribosomal diseases or ribosomopathies. Understanding the mechanisms linking ribosome biogenesis and cell cycle control in human requires a better understanding of pre-ribosome maturation in mammalian cells.

In eukaryotes, four ribosomal RNAs (rRNAs) constitute the ribosome: the 18S rRNA in the small 40S ribosomal subunit and the 5.8S, 28S and 5S rRNAs in the large 60S subunit. These RNAs are synthesized from two genes, as the 18S, 5.8S and 28S rRNAs are included in a polycistronic transcript, the 47S pre-ribosomal RNA (pre-rRNA), generated by RNA polymerase I from the ribosomal DNA; the 5S rRNA is produced by RNA polymerase III from a specific transcription unit. The ribosomal genes are highly repeated and form clusters around which the nucleoli organize in the nucleus. Nascent pre-rRNAs assemble co-transcriptionally with ribosomal proteins and *trans*-acting factors, forming large ribonucleoproteic particles called pre-ribosomes. RNA folding and cleavage, nucleotide enzymatic modifications and ribosomal protein assembly gradually transform these

*To whom correspondence should be addressed. Tel: +33 5 61 33 59 26; Fax: +33 5 61 33 58 86; Email: gleizes@ibcg.biotoul.fr
Present address:
Valérie Choesmel, LBCMCP, UMR5088, CNRS, 118 route de Narbonne, F-31062 Toulouse, France and Université de Toulouse, 31000 Toulouse, France.

early particles into mature ribosomal subunits, which involve the concerted activity of most of the 79 ribosomal proteins, >150 *trans*-acting proteins and 70 snoRNPs in yeast (9–11).

The yeast *Saccharomyces cerevisiae* has been the gold standard for defining the mechanisms of ribosomal RNA processing. Several cleavage sites have been precisely mapped in the external (ETS1, ETS2) and internal (ITS1, ITS2) transcribed spacers, which flank the mature ribosomal RNAs in the pre-rRNA (Figure 1) and are eliminated through several endo- and exonucleolytic steps (12). However, recent studies have shown that, beyond some common features, there was no straightforward relationship between yeast and mammalian pre-rRNA maturation. This is particularly true for processing of the ITS1 during maturation of the 18S rRNA

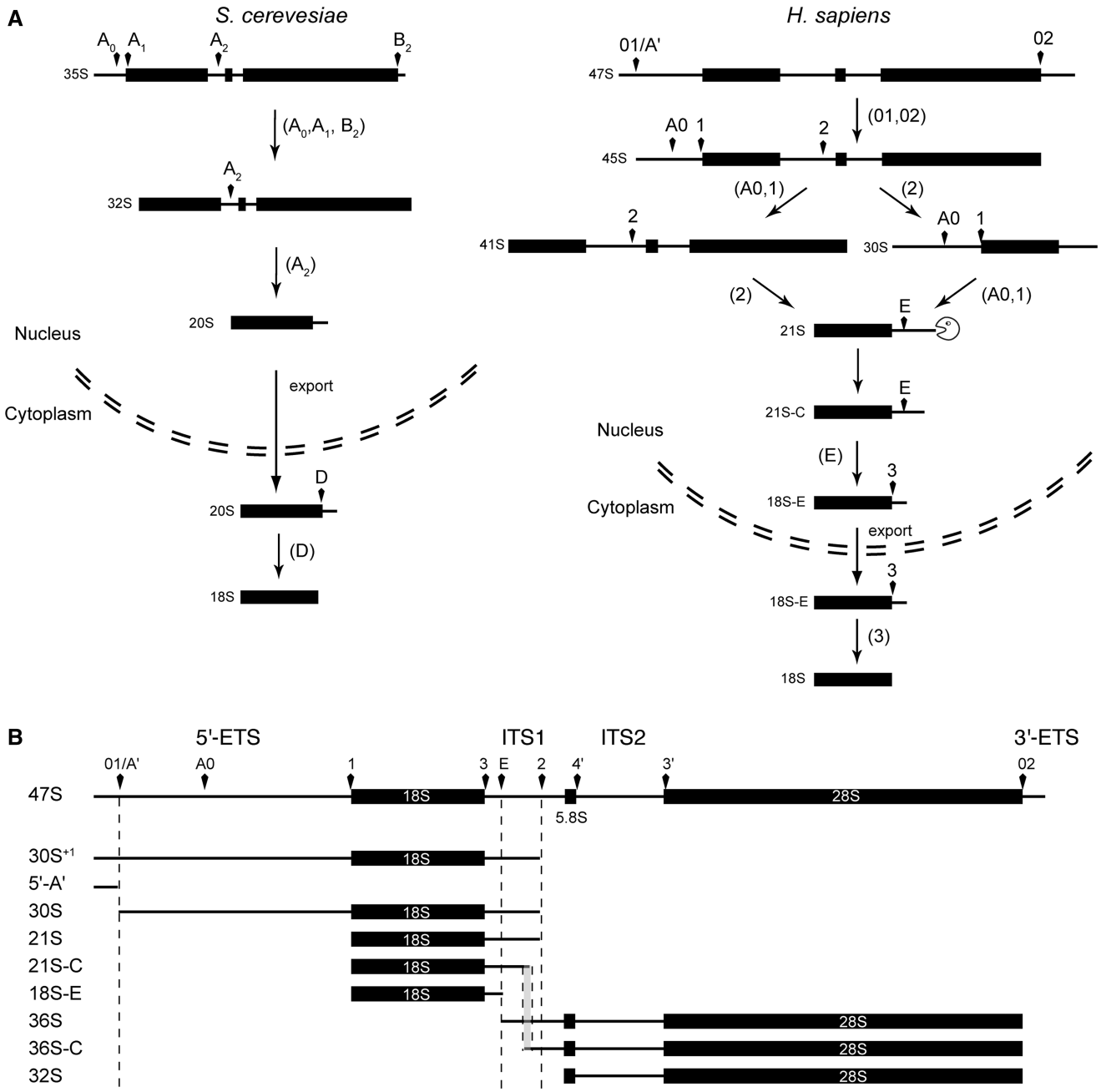

Figure 1. Processing of the pre-ribosomal RNAs. (**A**) Maturation of the 18S rRNA in yeast *S. cerevisiae* and in human cells. In vertebrate cells, the relative order of 5′-ETS elimination (cleavage sites A_0 and 1) and ITS1 cleavage at site 2 results in alternative pathways, which are characterized by the presence of either 41S or 30S pre-rRNAs. The 30S pre-rRNA is more abundant than the 41S pre-rRNA in HeLa cells, indicating that the corresponding pathway is predominant. In yeast, ITS1 is first cleaved at site A_2, this step is usually described as a post-transcriptional event (as presented here), but it may also occur co-transcriptionally. The nomenclature for the human pre-rRNA cleavage sites is adapted from previous studies (13–15). (**B**) Position of the pre-rRNA processing intermediates discussed in this article. The gray box common to the 21S-C and the 36S-C species corresponds to the highly conserved region referred in the text as C-region (Supplementary Figure S2).

(Figure 1). We have shown that processing of the ITS1 in human cells starts in the nucleolus and ends in the cytoplasm (13), as previously established in yeast. Nevertheless, it requires three endonucleolytic steps (cleavage at site 2, E and 3) (13), whereas only two are necessary in yeast (cleavage at site A_2 and D), as illustrated in Figure 1. Furthermore, loss-of-function experiments in HeLa cells of the pre-ribosomal factor Bystin/ENP1, or of the ribosomal protein RPS19, have revealed the potential involvement of a 3′–5′ exonuclease in the processing of the human ITS1 in the 21S pre-rRNA (Figure 1) (14). Finally, although initial endonucleolytic cleavage of the ITS1 at site A_2 in yeast is dependent on elimination of the ETS1 by cleavage at sites A_0 and A_1, the relative order of the cleavage of the 5′-ETS (ETS1) and the ITS1 is flexible in vertebrate cells, leading to several maturation pathways defined by specific processing intermediates (Figure 1) (15,16). Noticeably, mutations in DBA affect ITS1 processing in a large proportion of cases, especially after mutation of the small ribosomal subunit protein genes *RPS19* (17–19), *RPS26* (20), *RPS10* (20) and *RPS17* (21), but also of the large subunit protein gene *RPL26* (22).

Here, we have investigated the mechanisms of ITS1 processing in HeLa cells by focusing on the formation of the 18S-E pre-rRNA, the last precursor to the 18S rRNA. The 18S-E pre-rRNA is generated in the nucleolus and exported to the cytoplasm where the 18S 3′-end is generated. Our results show that conversion of the 18S-E pre-rRNA to the 18S rRNA is a multi-step process, which first involves endonucleolytic cleavage at site E, defined here ~80 nt downstream of the 18S 3′-end, and then 3′–5′ exonucleolytic trimming. This exonucleolytic processing gradually takes place between the nucleolus and the cytoplasm. In addition, endonucleolytic cleavage at site E is also followed by 5′–3′ exonucleolytic degradation by XRN2. This step may be mostly involved in the degradation of the excised ITS1, but it also defines a minor pathway for ITS1 removal in the 60S ribosomal subunit maturation. These data cast a new light on the mechanisms of pre-rRNA maturation in mammalian cells and show the unanticipated involvement of exonucleolytic processing in 18S rRNA formation in mammalian cells.

MATERIALS AND METHODS

Cell culture and knockdown of gene expression with small interfering RNAs

HeLa cells were cultured in Dulbecco's modified Eagle's medium supplemented with 10% fetal bovine serum and 1 mM sodium pyruvate. Ten microliters of a 100 μM siRNA solution (Eurogentec, Seraing, Belgium) was added to the cell suspension (10^7 cells in serum-free medium), and electro-transformation was performed with a Gene Pulser at 250 V and 950 μF in a 4-mm cuvette (Bio-Rad, Hercules, CA, USA). Different 21 mer siRNAs, whose efficiency was verified by quantitative polymerase chain reaction (qPCR), were used to knockdown expression of the following human protein genes: *RPS10* (GenBank accession number: NM_001014): 5′-GAACCG GAUUGCCAUUUAUdTdT-3′ (siRNA *rps10*); *RPS15* (GenBank accession number: NM_001018): 5′-UCACCU ACAAGCCCGUAAAdTdT-3′ (siRNA *rps15*); *RPS20* (GenBank accession number: NM_001023): 5′-GGUGU GUGCUGACUUGAUAdTdT-3′ (siRNA *rps20*); *RPL26* (GenBank accession number: NM_000987): 5′-GTCCAG GTTTACAGGAAGAdTdT-3′ (siRNA *rpl26*); *PES1* (GenBank accession number: NM_014303): 5′-GGCCTT GAGAAGAAGAAGTdTdT-3′ (siRNA *pes1*); *RIO2* (GenBank accession number: NM_018343): 5′-ACAUGG UGGCUGUAAUAAAdTdT-3′ (siRNA *rio2*); *XRN2* (GenBank accession number: NM_012255.3): 5′-GCCTA CCATTCACATTTGAdTdT-3′ (siRNA *xrn2*); *NOB1* (GenBank accession number: NM_014062.2): a mixture of 5′-CGCCCUGGAGCCAAUCUUCAAdTdT-3′ (siRNA *nob1Q1*), 5′-UUGCCCAACAUCGAUCAUGA AdTdT-3′ (siRNA *nob1Q2*) and 5′-UUGCCCAACAUC GAUCAUGdTdT-3′ (siRNA *nob1E3*). Experiments on transfected cells were performed 48 h after transfection of the siRNAs, except for hNOB1 knockdown, in which case the cells were treated for 6 days with siRNAs (three transfections at Day 0, 2 and 4). Control cells were electro-transformed with a scramble siRNA (siRNA-negative control duplex; Eurogentec). Anti-RRP6 and anti-hNOB1 antibodies were kindly provided by Dr Dominique Weil (CNRS, Paris) and Dr Ulrike Kutay (ETH Zürich), respectively.

Cell fractionation

Cells were removed by trypsin treatment and washed successively with phosphate-buffered saline and buffer A (10 mM HEPES, pH 7.9, 1.5 mM $MgCl_2$ and 10 mM KCl). Mechanical disruption was performed with a Dounce homogenizer in buffer A supplemented with 0.5 mM DTT, and 1/20 of total volume was used for total RNA extraction. After centrifugation at 1000*g* for 10 min at 4°C, the supernatant (cytoplasmic fraction) was recovered, and the nuclei-containing pellet was washed with 10 mM Tris–HCl, pH 7.5, 3.3 mM $MgCl_2$ and 250 mM sucrose. After centrifugation, the pellet was suspended in 10 mM $MgCl_2$ and 250 mM sucrose and purified by centrifugation (500*g* for 10 min, 4°C) on a sucrose cushion (0.5 mM $MgCl_2$ and 350 mM sucrose). To obtain nucleoplasmic and nucleolar fractions, 80% of the nuclear fraction was sonicated to disrupt nuclei. The nuclear suspension was separated by centrifugation (2000*g* for 10 min, 4°C) on a sucrose cushion (0.5 mM $MgCl_2$ and 880 mM sucrose). Two-thirds of the supernatant were recovered (nucleoplasmic fraction), and the pellet was washed with 10 mM Tris–HCl, pH 7.4, 2.5 mM $MgCl_2$ and 20 mM KCl. After centrifugation, the pellet was suspended in 10 mM Tris–HCl, pH 7.4, 10 mM NaCl and 10 mM DTT and kept at 15°C for 40 min under mild stirring. After sonication and centrifugation at 10 000*g* for 10 min at 16°C, the supernatant corresponding to the nucleolar fraction was recovered. RNAs were extracted with Tri Reagent (Molecular Research Center, Inc.) and dissolved in formamide at final concentration of 1 μg/μl.

RNase protection and 3′-RACE analysis

The probe was synthesized and labeled by *in vitro* transcription with T7 RNA polymerase (Promega, Charbonnières, France) in the presence of α^{32}P-CTP (cytidine triphosphate). Transcription products were verified on a 6% polyacrylamide gel containing 7 M urea. Two micrograms of RNA was incubated overnight at 50°C with 250 000 cpm of the probe in 10 µl of 40 mM piperazine-N,N′-bis(2-ethanesulfonic acid) (PIPES), pH 6.7, 400 mM NaCl, 1 mM ethylenediaminetetraacetic acid and 80% formamide. One hundred microliters of 10 mM Tris–HCl, pH 7.5, 200 mM NaCl, 5 mM ethylenediaminetetraacetic acid, 100 mM LiCl and 1.5 µl of RNases A/T1 mix (Promega) were added to the solution, and digestion was carried out for 45 min at 30°C. The reaction was stopped by addition of 2 µl of 10% sodium dodecyl sulfate (SDS) and 20 µg of proteinase K (Sigma, Saint-Quentin Fallavier, France) followed by a 15 min incubation at 37°C. After phenol extraction and ethanol precipitation, digestion products were suspended and loaded onto an 8% polyacrylamide gel containing 7 M urea. After migration, the gel was dried and exposed. Signals were acquired with a PhosphorImager (FLA2000, Fuji, Stamfort, CT, USA) and quantified using the ImageGauge software.

The 3′-RACE (Rapid Amplification of cDNA Ends) analysis was adapted from Kiss and Filipowicz (23). Primer ITS1-Hs-RACE (5′-CGCGAATTCGATCATTA ACGGAGCCCGGAG-3′), which spans the 18S-ITS1 junction up to nucleotide 11 in the ITS1, was used for PCR amplification. The amplified fragments were sub-cloned and automatically sequenced.

Northern blot

Three micrograms of total RNAs was separated on a 1.2% agarose gel containing 1.2% formaldehyde and 1× Tri/Tri buffer (30 mM triethanolamine and 30 mM tricine, pH 7.9). RNAs were transferred to Hybond N^+ nylon membrane (GE Healthcare, Orsay, France) by passive transfer and cross-linked under ultraviolet light. Membrane pre-hybridization was performed at 45°C in 6× SSC (saline-sodium citrate), 5× Denhardt's solution, 0.5% SDS and 0.9 µg/ml tRNA. The 5′-radiolabeled oligonucleotide probe was added after 1 h and incubated overnight at 45°C. The pre-hybridization and hybridization temperatures were raised to 65°C for the ITS1-38, ITS1-49, ITS1-59 and ITS1-78 probes. Membranes were washed twice for 10 min in 2× SSC and 0.1% SDS and once in 1× SSC and 0.1% SDS, and then exposed.

Primer extension

Reverse transcription was performed using the ThermoScript^{TM} reverse transcriptase–PCR system (Invitrogen, Paisley, UK). Four micrograms of total RNA was incubated with 50 000 cpm of radiolabeled primer for 5 min at 65°C and then chilled on ice. cDNA synthesis was carried out under the manufacturer's conditions for 1 h at 60°C. The reaction products were precipitated and suspended in formamide loading buffer. Sequencing reactions were performed using the Thermo-Sequenase Cycle Sequencing kit (USB-Affymetrix, Temse, Belgium) as indicated by the manufacturer. One half of each reaction was loaded onto a 10% polyacrylamide gel containing 7 M urea. After migration, the gel was dried and exposed.

Probes

The sequences of the probes used for northern blot and/or primer extension were: 5′-ITS1 (5′- CCTCGCCCTCCGG GCTCCGTTAATGATC-3′), ITS1-38 (5′- GGAGGGAA GCGCGCGGCGGC-3′), ITS1-49 (5′-GGTGGGTGTG CGGAGGGAAG-3′), ITS1-59 (5′-GCGGTGGGGGGG TGGGTGTG-3′), ITS1-78 (5′-GCCCGCGCACGCGCC GCGTCG-3′), ITS1-102 (5′-GAACGAACGGGCACGC GGGC-3′), ITS1-565 (5′-GCGGGGGGGCGGACGAG GAG-3′), ITS1-598 (5′-TCCGCGCCGGAACGCGCT AG-3′), ITS1-721 (5′-GGAGCGGAGTCCGCGGTG GAG-3′), ITS1-815 (5′-ACGGCACACGCGCGGCAG GC-3′), 5′-ETS-b (5′-AGACGAGAACGCCTGACACG CACGGCAC-3′), 18S (5′-TTTACTTCCTCTAGATAG TCAAGTTCGACC-3′), ITS2 (mix of 5′-CTGCGAGG GAACCCCCAGCCGCGCA-3′ and 5′-GCGCGACGG CGGACGACACCGCGGCGTC-3′) and 28S (5′-CCCG TTCCCTTGGCTGTGGTTTCGCTAGATA-3′).

RESULTS

Cleavage at site E is followed by 5′–3′ exonucleolytic processing of the ITS1

The 36S pre-rRNA is the precursor resulting from direct endonucleolytic cleavage at site E of the 45S pre-rRNA (Figure 1B). Direct cleavage of the ITS1 at site E is a minor pathway in HeLa cells, as indicated by the very low levels of 36S pre-rRNA relative to the 30S and 21S pre-rRNAs (Figure 2B and C, lane 1), which results from initial cleavage of the ITS1 at site 2 (14). In contrast, the 36S intermediate is commonly observed in rodent cells (24), which indicates different kinetics of cleavage at sites E and 2 (also called 2b and 2c in mouse) compared with human cells. It was recently shown that the 36S pre-rRNA is a substrate for the XRN2 exonuclease in mouse cells (24). Similarly, we observed that knockdown of XRN2 in HeLa cells triggered accumulation of 36S pre-rRNA (Figure 2B and C, lane 4; see quantification in Supplementary Figure S1). In parallel, a low molecular weight band was detected with probes hybridizing around positions 78 and 721 in the ITS1 (Figure 2B and C, lane 4). This band likely corresponds to the E-2 fragment produced by endonucleolytic cleavage of the 21S pre-RNA at site E. Accumulation of this fragment on XRN2 knockdown suggests that it is normally trimmed by XRN2. The levels of 41S and 21S pre-rRNAs were comparable with control, indicating that accumulation of 36S pre-rRNA was not because of defective cleavage at site 2. The amount of 30S pre-rRNA was reduced on XRN2 depletion, but we observed the appearance of the $30S^{+1}$ pre-rRNA. This precursor results from cleavage at site 2 without early cleavage of the 5′-ETS at site A′ (Figure 1A and B). Accordingly, it was also detected

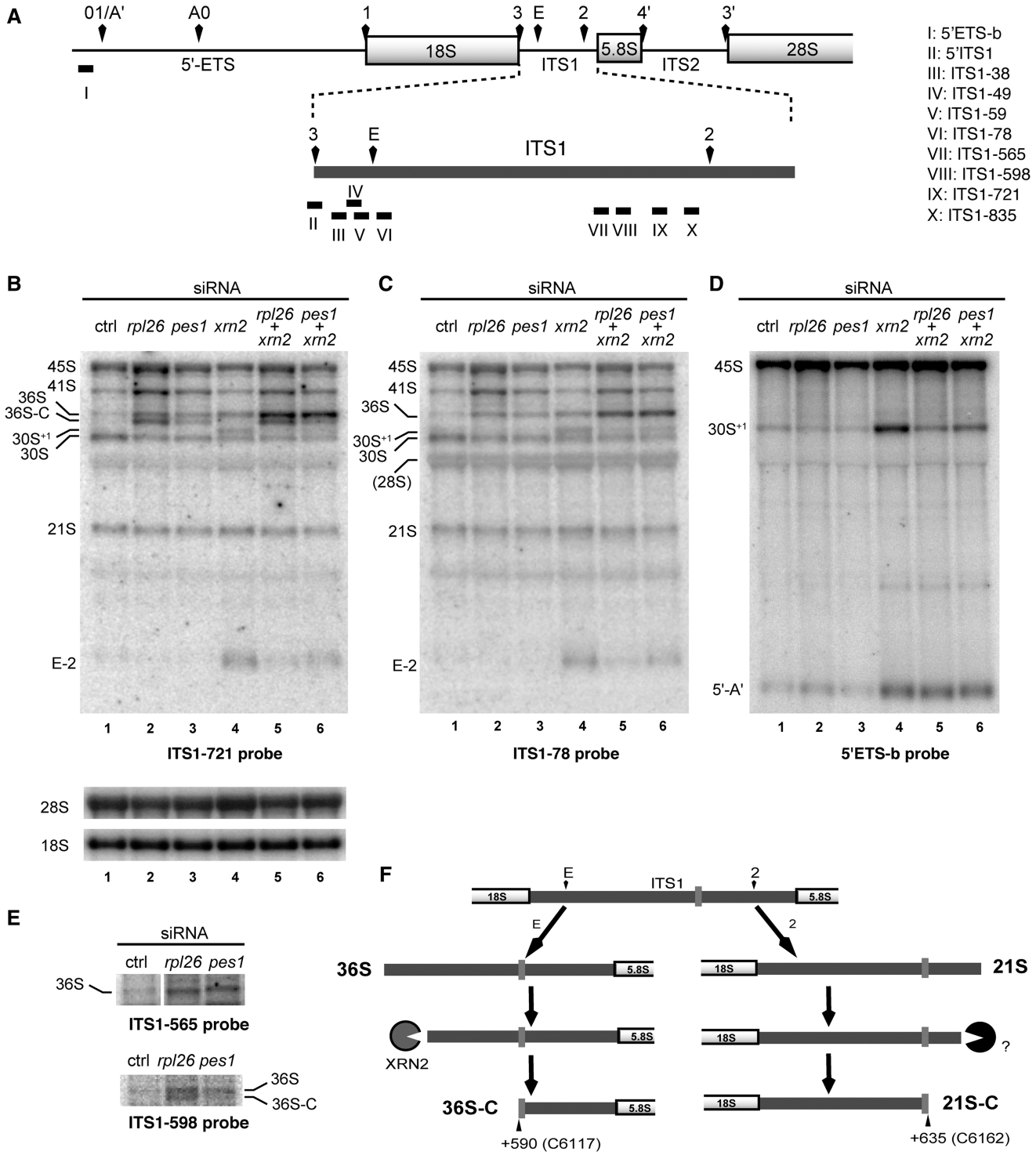

Figure 2. Exonucleolytic processing of the ITS1 by XRN2 is perturbed by RPL26 or PES1 knockdown. (**A**) Position on the pre-rRNA of the hybridization probes used in the present work. (**B–E**) Northern blot analysis of pre-rRNAs in HeLa cells after knockdown of RPL26, PES1 or XRN2. (B) The ITS1-721 probe reveals increased levels of the 36S pre-rRNA in siRNA-treated cells, as well as the new 36S-C species in RPL26- and PES1-depleted cells. (C) Hybridization with the ITS1-78 probe reveals the fast migrating band observed in panel B, indicating that it corresponds to the E-2 fragment. The probe shows non-specific cross-hybridization with the 28S rRNA. (D) Hybridization with the 5′-ETS-b probe shows accumulation of the $30S^{+1}$ precursor in XRN2-depleted cells. Accumulation of the 5′-A′ fragment is also detected. (E) The 36S-C pre-rRNA accumulating on RPL26 and PES1 knockdown is not detected with the ITS1-565 probe (top panel), but it hybridizes with the ITS1-598 probe (bottom panel). (**F**) Schematic representation of exonucleolytic processing of the ITS1 based both on the previously described data and on previous results on processing of the 21S pre-rRNA (14). In the absence of RPL26 and RPS19, respectively, 5′–3′ processing of the 36S RNA or 3′–5′ processing of the 21S pre-rRNA are stalled on both sides of a highly conserved region of the ITS1 (C-region), represented as a light grey box.

with the 5′-ETSb probe that hybridizes upstream of the 01/A′ site (Figure 2D, lane 4) (25). Overall, the cumulative amount of 30S and $30S^{+1}$ pre-RNAs corresponded to the amount of 30S pre-rRNA in control cells, confirming that cleavage at site 2 was not affected. The accumulation of 36S pre-rRNA and of the E-2 fragment on XRN2 knockdown indicates that cleavage at site E in human cells is normally followed by 5′–3′ exonucleolytic trimming of the ITS1 by XRN2.

A highly conserved cis-acting element involved in the control of ITS1 processing

We have recently reported that depletion of ribosomal protein RPL26 in HeLa cells blocks cleavage at site 2, but not cleavage at site E, as indicated by accumulation of 18S-E and 36S pre-rRNAs and decreased levels of 21S and 30S pre-rRNAs [(22); Figure 2B and C, lane 2]. In addition, using a probe complementary to the core of the ITS1, we observed a band migrating just below the 36S pre-rRNA (Figure 2B, lane 2). Assembly of Rpl26p in pre-ribosomes in *S. cerevisiae* was shown to require Nop7p, the yeast homolog of human PES1 (26). Accordingly, HeLa cells treated with siRNAs targeting expression of PES1 displayed a phenotype similar to that observed in RPL26-depleted cells (Figure 2B, lane 3). By northern blot analysis, we localized the 5′-end of the lower migrating species between nucleotides +570 and +602 of the ITS1 (Figure 2E). Primer extension experiments showed arrests around position +590 in cells treated with the siRNAs *rpl26* (data not shown). We named this species 36S-C (corto is the Italian for short). When PES1 or RPL26 were co-depleted with XRN2, we observed an increase in 36S pre-rRNA, whereas the amount of 36S-C RNA slightly decreased (Figure 2B, lanes 5 and 6). No fragment extending from site E to the 5′-end of the 36S-C RNA was detected, unlike what would be expected from endonucleolytic cleavage of the 36S pre-rRNA. This result suggests that exonucleolytic processing of the 36S pre-rRNA is stalled or delayed around position +590 in the ITS1, giving rise to the 36S-C RNA. Noticeably, the 5′-end of the 36S-C RNA is located in the same region as the 3′-end of the 21S-C intermediate, which putatively arises from 3′ to 5′ exonucleolytic trimming of the 21S pre-rRNA (14). We found that the 45 nt region delineated by the 5′-end of the 36S-C pre-RNA and the 3′-end the 21S-C pre-RNA corresponds to the most conserved segment in the ITS1 of mammals (Supplementary Figure S2). This region might control the progression of exonucleases that trim the ITS1 after endonucleolytic cleavage at sites E and 2 (Figure 2F).

Mapping of site E

Cleavage at site E generates the 18S-E and the 36S pre-rRNAs. This site has not been precisely mapped. We took advantage of the accumulation of 36S pre-rRNA in cells depleted of XRN2 to localize site E. By northern blot, we detected the 18S-E pre-rRNA and not the 36S pre-rRNA with the ITS1-38 probe (Figure 3A), which hybridizes between nucleotides +38 and +57 in the ITS1 (Figure 3C). In contrast, the ITS1-78 probe spanning the +78 to +98 segment detected the 36S RNA and the E-2 fragment in XRN2-depleted cells but not the 18S-E pre-rRNA (Figure 3A). The 5′-end of the 36S RNA was then mapped by primer extension, with a probe complementary to nucleotides +102 to +121. Consistent with the northern blot data, we identified two extension arrests that were stronger after XRN2 knockdown at nucleotides G5606 (+79) and G5609 (+82) (Figure 3B). Reciprocally, when 3′-RACE experiments were performed to determine the 3′-end of the 18S-E, the longest RNA detected ended at position C5605 (+78) in several independent experiments (see dashed bars in Figure 5A in the nuclear and cytoplasmic fractions and in Figure 6A for RPS20 and RPS15 knockdown). RNAs ending at position C5608 (+81) were also detected in two independent experiments (see dashed bars in Figure 5A in the nucleolar fraction and in Figure 6A for RIO2 knockdown). We conclude from these data that endonucleolytic processing of the ITS1 at site E corresponds to two cleavages after nucleotides C5605 (+78) and C5608 (+81) (Figure 3C).

The 18S-E pre-rRNA exists under several forms

The 3′-RACE experiments performed to determine the extremity of the 18S-E pre-rRNA delivered a much more complex picture than previously envisioned (13), as illustrated in Figure 4A, as well as in Figures 5A and 6A. We observed multiple extremities, which suggest that the 18S-E pre-rRNA undergoes 3′–5′ exonucleolytic maturation after cleavage at site E. As described previously (13), a fraction of RNAs ending around G5551 (position +24 of ITS1) was detected (Figure 4A). In addition, we found another set of extremities between G5562 and C5567 (+35 to +40 in the ITS1), which are collectively named '18S-E/36' in the rest of the text. Less than 10% of the RNAs ended after positions +58. The low abundance of these longer forms likely explains why probes covering the +58 to +78 segment (the ITS1-49 and ITS1-59 probes) did not detect the 18S-E pre-rRNA (Figure 3A). To confirm the presence of several 18S-E species, we performed RNase protection on total RNAs with a probe spanning the last 87 nt of the 18S rRNA and the first 63 nt of the ITS1 (see schematic in Figure 4B). As control templates, we used *in vitro* transcribed RNA fragments corresponding to the last 87 nt of the 18S rRNA followed by the first 24 or 36 nt of the ITS1 (Figure 4B, lanes 2 and 3). Five bands (visualized as doublets or triplets for undetermined reasons) were detected on total RNAs (Figure 4B, lane 1). As expected, the most intense band corresponded to the 18S rRNA. In addition, two bands could be distinguished around positions +24 and +36. Protection of the entire probe yielded the slowest migrating fragment. The fastest migrating band likely corresponds to a fragment of the 18S rRNA segment shortened on the 3′-end, as a radioactive probe spanning only the last 55 nt of the 18S rRNA gave a similar pattern with all the bands shifted towards the bottom of the gel (Supplementary Figure S3B), indicating that the five bands contained the 18S rRNA nucleotides. Based on the 3′-RACE experiments, we could exclude the possibility

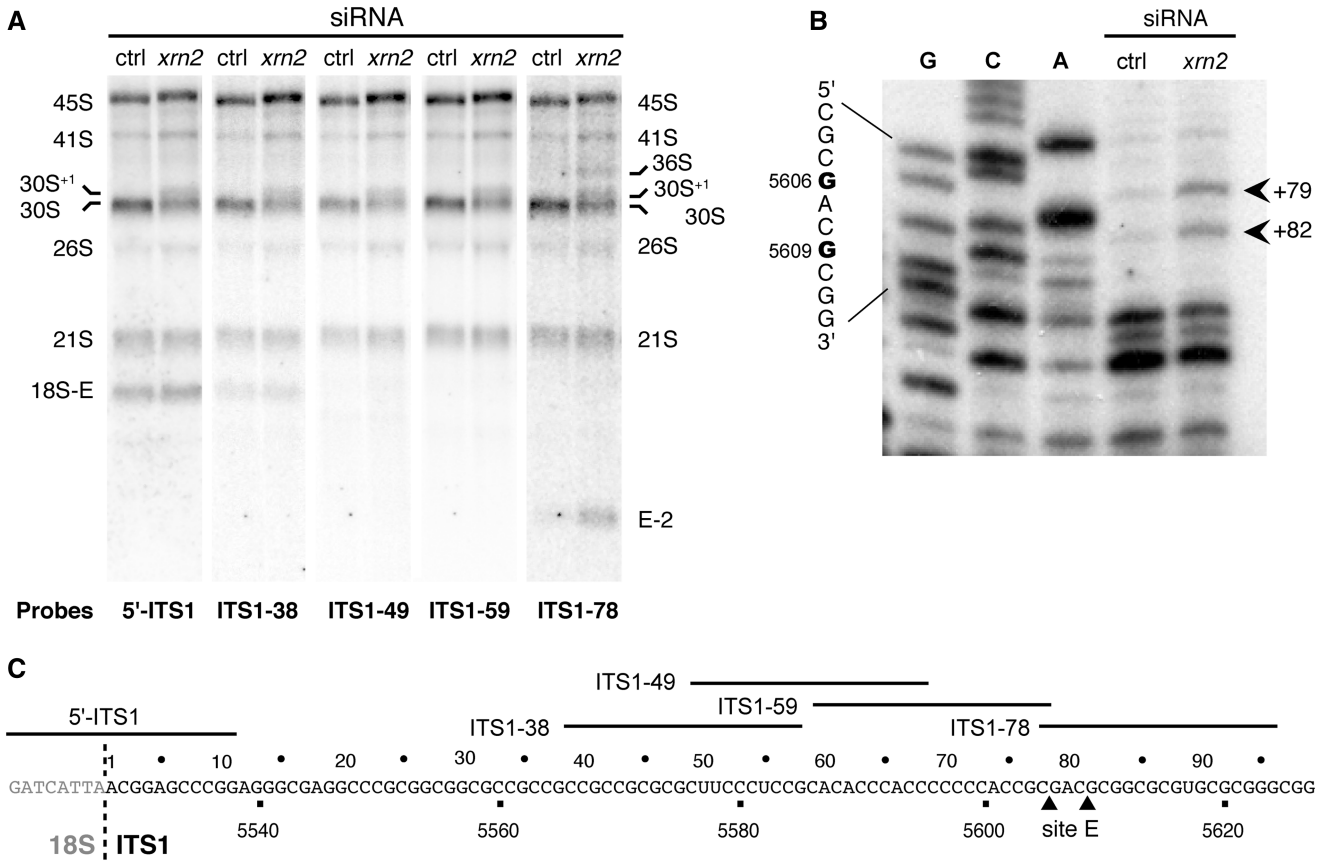

Figure 3. Mapping of site E. (**A**) Northern blot analysis of pre-rRNAs in control and XRN2-depleted cells. The ITS1-38 probe detects the 18S-E pre-rRNA, whereas the ITS1-78 detects the 36S pre-rRNA. The ITS1-49 and ITS1-59 probes detect neither of these species under these conditions. (**B**) Primer extension analysis of the 36S 5′-end in control and XRN2-depleted cells. The ITS1-102 oligonucleotide was used for reverse transcription. Arrowheads show two arrests that are enhanced in RNAs from XRN2-depleted cells, corresponding to nucleotides G5606 and G5609. (**C**) Schematic representation of probe hybridization sites on ITS1. Arrowheads indicate the cleavage positions for site E. The numbering relative to the rDNA transcription start site is indicated below the sequence.

that this fast migrating band was an alternative 3′-end of the 18S rRNA (Supplementary Figure S3D), and we hypothesize that it corresponds to an experimental artefact. Taken together, the 3′-RACE and the RNase protection data show that the 18S-E pre-rRNA is present as different species, which are likely to correspond to sequential steps in the exonucleolytic processing of the 18S-E pre-rRNA after cleavage at site E.

The 18S-E pre-rRNA is gradually matured from the nucleolus to the cytoplasm

The 18S-E pre-rRNA is formed in the nucleolus and exported to the cytoplasm, where it is maturated into 18S rRNA (13). To understand the temporal relationship between 3′–5′ exonucleolytic processing and nuclear export of the 18S-E pre-rRNA, we performed nucleus–cytoplasm fractionation and analyzed the RNAs from each fraction by 3′-RACE and RNase protection. The 3′-RACE experiments revealed a majority (60–70%) of long species extending beyond position +40 in the nucleolar fraction of HeLa cells (Figure 5A). In contrast, such species represented <10% of the clones amplified from the cytoplasmic fraction. The whole-nucleus fraction displayed an intermediate situation. The nucleolar and nuclear fractions contained 20–30% of fragments ending between positions 42 and 45. These species were much less abundant in the cytoplasm, where we observed accumulation of shorter pre-RNAs ending at positions +14 and +24, as well as a fraction of pre-RNAs with ends spreading between +35 and +42. The presence of the longest 18S-E species in the nucleolar and the nuclear fraction was supported by RNase protection experiments (Figure 5B and Supplementary Figure S3B). As expected, RNase protection experiments also showed that the 18S rRNA was poorly detected in the nucleolar fraction but was strongly present in the cytoplasmic fraction and to some extent in the nucleoplasmic fraction because of cytoplasmic contamination (Figure 5B). This mature 18S rRNA likely competes with the 18S-E pre-rRNA for binding to the probe, which weakens the signal of the 18S-E pre-rRNA in these fractions. RNase protection performed on cellular fractions from U2OS cells gave similar results (Supplementary Figure S3C).

The presence of intermediate forms of the 18S-E pre-rRNAs in the cytoplasmic fraction shown by 3′-RACE suggests that release from the nucleolus and nuclear export can take place rapidly after cleavage at site E. However, the asymmetric distribution of the long and short forms of the 18S-E pre-rRNA between the

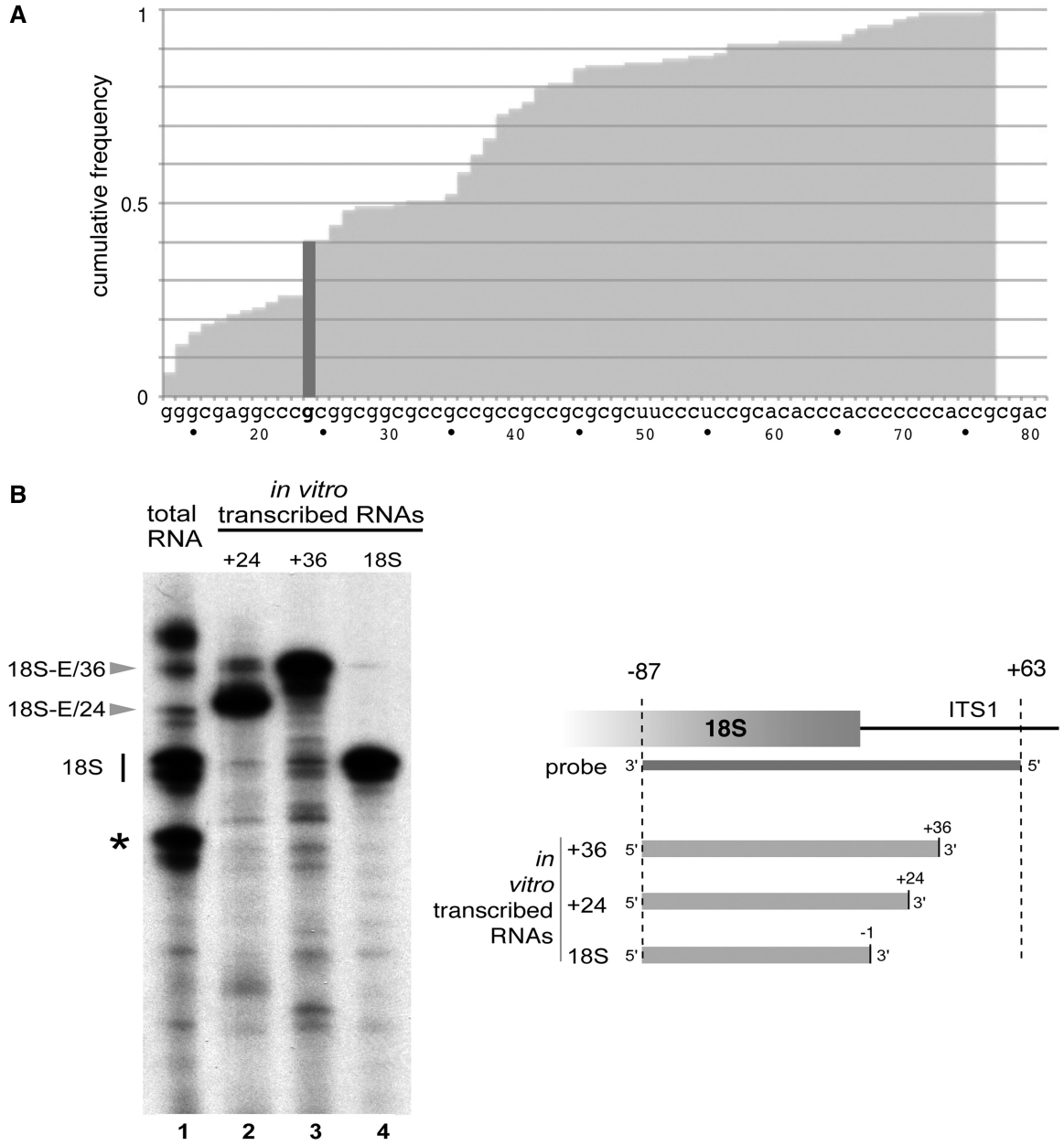

Figure 4. Analysis of the 3′-end of the 18S-E pre-rRNA reveals multiple forms. (**A**) Analysis by 3′-RACE of the 18S-E pre-rRNA in control cells ($n = 126$). In this cumulative plot, the bars correspond to the proportion of fragments ending at or before a given position. Each step in the graph can be read as the proportion of fragments with their 3′-end positioned at the corresponding nucleotide. Position +24 of the ITS1 is indicated in dark gray. (**B**) RNase protection analysis performed on cellular RNAs (lane 1) or *in vitro* transcribed RNA (lanes 2–4). The asterisk indicates an artefactual band (see 'Results' section and Supplementary Figure S3). The highest band likely corresponds to full protection of the probe (up to nucleotide +63 in the ITS1). We checked that the probe was fully digested in the absence of HeLa cell RNAs (Supplementary Figure S3A). The schematic shows the position of the probe and of the different *in vitro* transcribed RNAs relative to the pre-rRNA.

nucleolus and the cytoplasm strongly suggests that trimming of the 3′-end of the 18S-E RNA by exonucleolytic processing starts in the nucleolus and gradually proceeds during transport to the cytoplasm.

Depletion of progression ribosomal proteins of the small subunit (p-RPS) blocks final maturation of the 18S-E/24 pre-rRNA

We next investigated the relationship between the gradual maturation of the 18S-E pre-rRNA and the assembly of ribosomal proteins involved in the progression of the 18S rRNA maturation (p-RPSs) (25). On knockdown of ribosomal proteins RPS10 and RPS20 with siRNAs, two proteins whose depletion results in cytoplasmic accumulation of 18S-E pre-rRNA (25), 3′-RACE experiments showed a strong enrichment of fragments ending at nucleotide +24 in total RNAs (Figure 6A). Similar results were obtained on knockdown of kinase RIO2 (Figure 6A), a component of the pre-40S particle required for cytoplasmic conversion of the 18S-E pre-rRNA to 18S rRNA

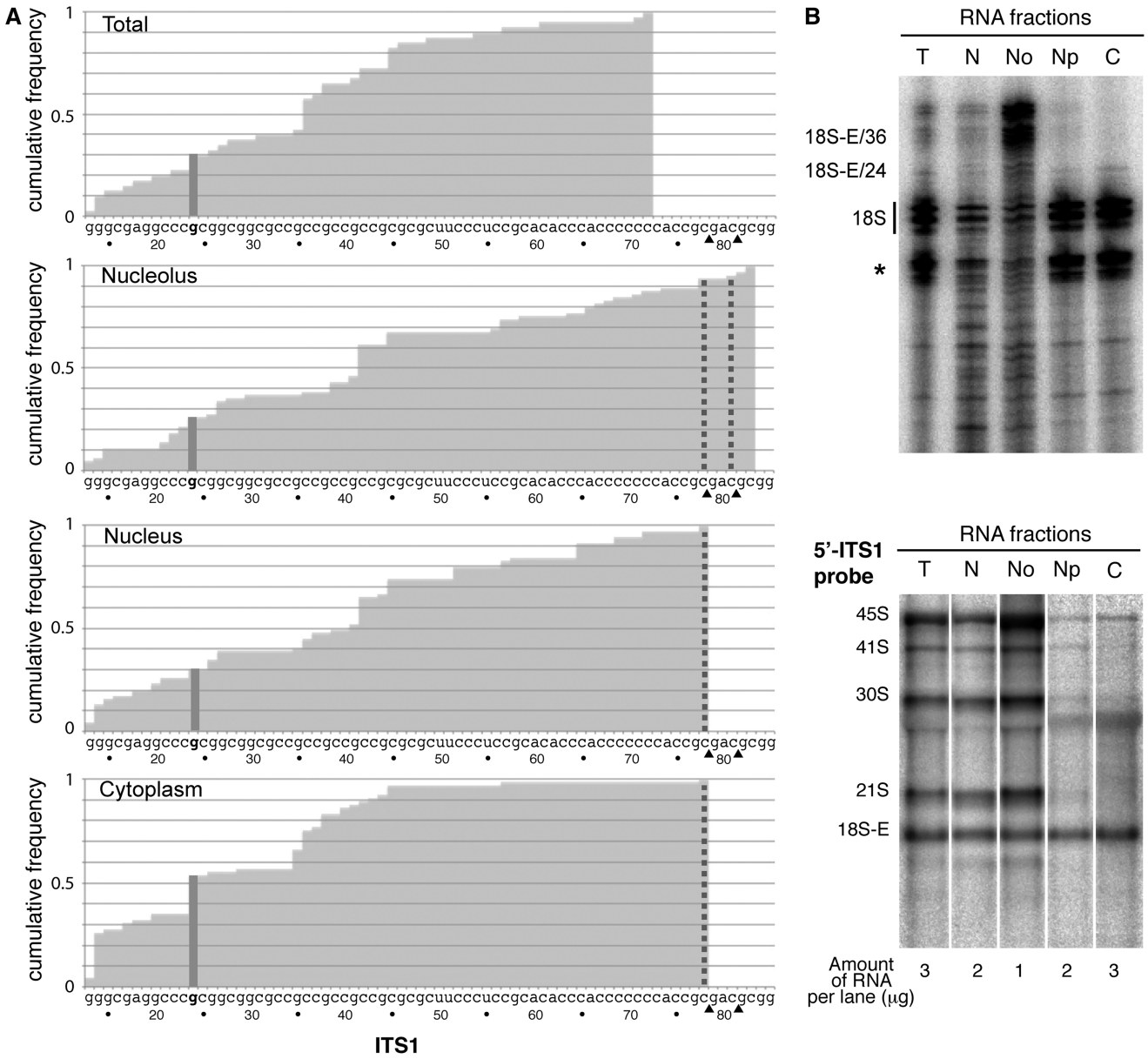

Figure 5. Intracellular distribution of the different forms of 18S-E pre-rRNA. (**A**) Analysis by 3′-RACE of the 18S-E pre-rRNA in total ($n = 40$), nucleolar ($n = 65$), nuclear ($n = 69$) and cytoplasmic ($n = 65$) RNAs. The arrowheads indicate the 5′-ends of the 36S pre-rRNA mapped by primer extension (Figure 3). Position +24 of the ITS1 is indicated in dark gray. The dashed bars indicate the presence of fragments expected from endonucleolytic cleavage after nucleotides +78 and +81. (**B**) RNase protection analysis (upper panel) performed on RNAs isolated from cellular fractions. The positions of the fragments indicating protection by the 18S rRNA and the 18S-E/24 and 18S-E/36 forms are indicated. The same amount of RNA was hybridized to the probe in the different fractions. The distribution of the 18S rRNA precursors in the fractions used for the RNase protection assay is shown in the lower panel. T: Total; N: Nucleus; No: Nucleolus; Np: Nucleoplasm; C: Cytoplasm.

(13,27). Consistently, we observed the accumulation of the 18S-E/24 intermediate on depletion of RPS10, RPS20 or RIO2 by RNase protection assay (Figure 6B and C). The 18S-E/24 intermediate accumulated in the cytoplasmic fraction, whereas the longer forms were more abundant in the nuclear fraction (Figures 6B and C). We next knocked down RPS15, which is required for nuclear export of the pre-40S particles (13,25). As for RPS10 and RPS20, absence of RPS15 did not block the exonucleotytic processing of the 18S-E pre-rRNA, as shown by 3′-RACE (Figure 6A). In this case, we observed a conspicuous accumulation of short forms of the 18S-E pre-rRNA in the nuclear fraction by RNase protection (Figure 6D), as expected from nuclear retention of pre-40S particles. Accumulation of the 18S-E RNA on knockdown of RPS10, RPS15, RPS20 and RIO2 was detected on northern blots with the 5′-ITS1 probe, which hybridizes with all forms of 18S-E pre-rRNA, but not with a probe detecting only the longest forms (Figure 6E). The longest forms did not accumulate either on depletion of RPS2 and RPS17, two p-RPSs partly required for nuclear export of the pre-40S particles (25). These data indicate

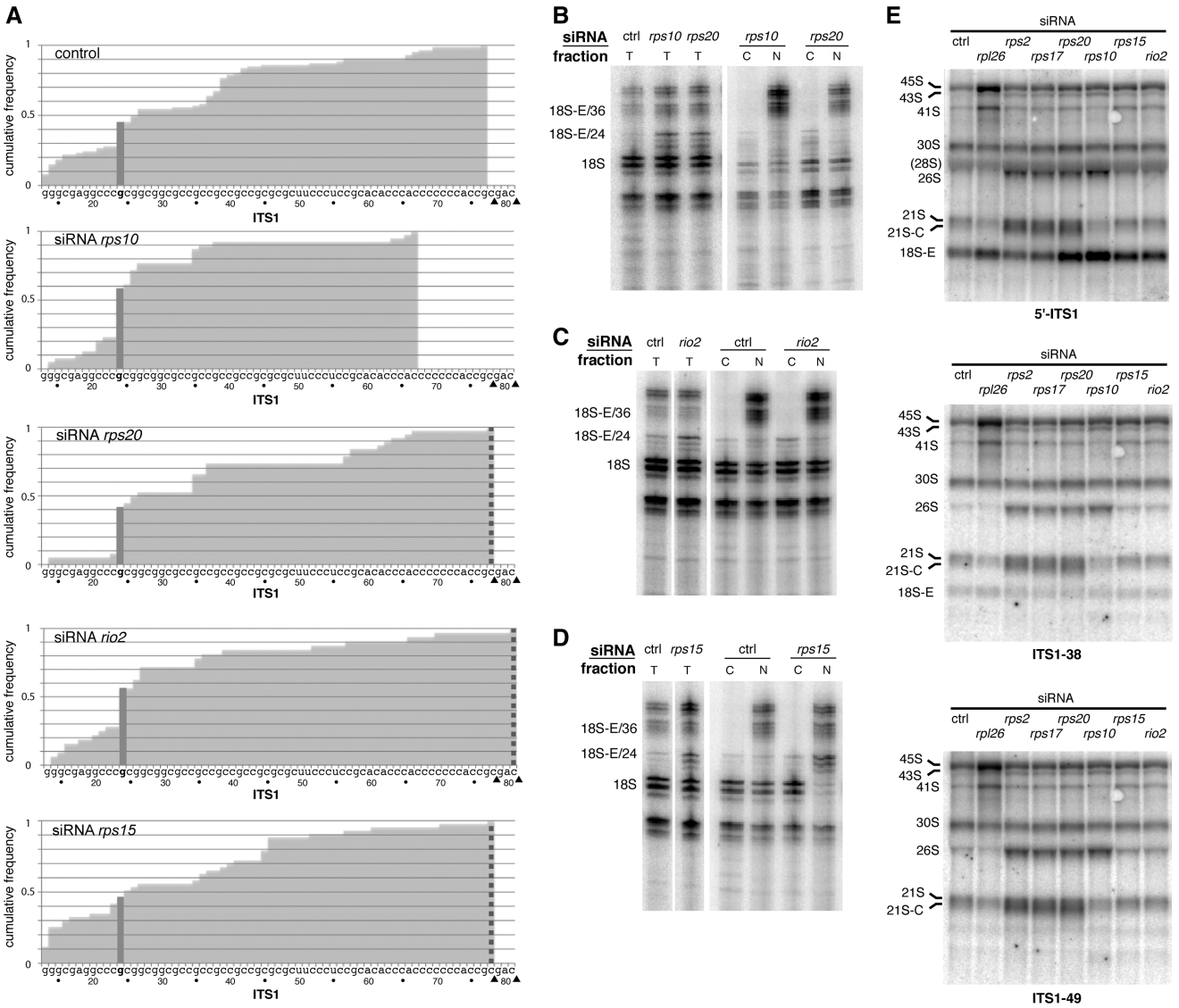

Figure 6. Analysis of the 3′-end of the 18S-E pre-rRNA in progression RPS-depleted cells. HeLa cells were transfected for 48 h with siRNAs knocking down RPS10, RPS20, RPS15 and RIO2. (**A**) The 3′-RACE analysis of the 18S-E pre-rRNA in control cells ($n = 86$) or in cells depleted of RPS10 ($n = 39$), RPS20 ($n = 38$), RIO2 ($n = 32$) and RPS15 ($n = 43$). Position +24 of the ITS1 is indicated in dark gray. The arrowheads indicate the endonucleolytic cleavage sites determined in Figure 3B, and the dashed bars correspond to the fragments expected from endonucleolytic cleavage at these positions. (**B–D**) RNase protection analysis was performed on total (T), cytoplasmic (C) or nuclear (N) RNAs extracted from cells depleted of RPS10 or RPS20 (B), RIO2 (C) or RPS15 (D). The same amount of RNA was hybridized to the probe in the different fractions. Positions of the fragments protected by the 18S rRNA, the 18S-E/24 or the 18S-E/36 intermediates are indicated. (**E**) Northern blot analysis of the 18S rRNA precursors shows accumulation of 18S-E pre-rRNA after knockdown of various proteins, including RPS10, RPS15, RPS20 and RIO2 (5′-ITS1 probe). However, long forms of 18S-E pre-rRNA do not accumulate (ITS1-38 and ITS1-49 probes). Similar results are obtained after knockdown of RPS2 and RPS17, which leads to partial retention of 18S-E pre-RNA in the nucleus like RPS15 depletion (25).

that exonucleolytic trimming of 18S-E pre-rRNA down to nucleotide +24 does not strictly depend on correct assembly of the pre-40S particles. Removal of the last 24 nt in turn represents a second step that is affected on loss of function of RIO2 or ribosomal proteins.

Function of the exosome and of hNOB1 in the maturation of the 18S-E pre-rRNA

The exosome is a large protein complex originally described in yeast *S. cerevisiae* as involved in the processing of rRNA precursors, especially 3′-end maturation of the 5.8S rRNA (28). It is also required for the degradation of misprocessed pre-rRNAs (29). The catalytic activity of the exosome complex is ensured by two 3′–5′ exoribonucleases, Rrp6p and Rrp44p (30,31), whose human counterparts, PM/Scl-100 (RRP6) and DIS3, are also associated to the exosome and located in the nucleus. A paralog of DIS3 called DIS3-like exonuclease 1 (hDIS3L1) has been described as a novel exosome-associated exoribonuclease, but it is located in the cytoplasm (32,33). Another DIS3 paralog, hDIS3L2, possesses exonucleolytic activity *in vitro*, but its association with the exosome is still unclear (34). To examine whether the

exosome plays a role in the exonucleolytic maturation of the 18S-E pre-rRNA, we knocked down expression of RRP6 and DIS3, and analyzed the pre-rRNAs by northern blot. Knocking down RRP6 triggered a strong accumulation of 21S-C pre-RNA (Figure 7A). In addition, new bands were detected with probes ITS1-38, ITS1-49 and ITS1 59, which should recognize the long forms of the 18S-E pre-rRNAs (bands 'a' and 'b' in Figure 7A). Band 'a' suggested accumulation of a long form of 18S-E pre-rRNA. But as these bands were also detected with probes ITS1-78 and ITS1-815, we conclude that they likely correspond to aberrant precursors or to degradation intermediates containing a major part of the ITS1. Accordingly, no obvious accumulation of long forms of 18S-E pre-rRNA was observed by 3′-RACE or RNase protection (data not shown). Depletion of RRP6 also resulted in accumulation of 12S pre-rRNA and 5.8S precursors, consistent with previous results (33). Knockdown of DIS3 by two different siRNAs induced a modest decrease of the global level of the 18S rRNA precursors, except for the 21S pre-rRNA (Figure 7B). In contrast, conversion of the 12S pre-rRNA into 5.8S rRNA was clearly affected, indicating a role for DIS3 in the maturation of the 5.8S (33), similar to its yeast ortholog Rrp44p. Depletion of DIS3L1 or DIS3L2 did not seem to affect pre-rRNA processing (data not shown), which corroborates previous reports (33,34). These data suggest a potential role of the exosome, and more specifically RRP6, in the processing of the 21S pre-rRNA. However, processing of the 18S-E pre-rRNA seems to be ensured by other exonucleases.

Finally, we knocked down hNOB1, the human homolog of yeast endonuclease Nob1p, which catalyses the final cleavage at the 18S rRNA 3′-end (35). As shown in Figure 7C, the 18S-E pre-rRNA did accumulate after hNOB1 depletion, which supports the hypothesis that hNOB1 performs endonucleolytic cleavage at the 18S rRNA 3′-end similar to Nob1p in yeast.

The 18S-E pre-rRNA is poly-uridylated in the cytoplasm

The 18S-E pre-rRNA sequences obtained by 3′-RACE often presented extra nucleotides at their 3′-end (Supplementary Figure S4). We often observed an extra A, which we interpreted as an artefact because of the presence of free adenosine triphosphate during the first step of 3′-RACE. But most interestingly, we noticed that a large fraction of the sequences obtained from cells treated with siRNAs against RPS10 or RPS20 were frequently extended by 1–5 uridines (53 and 61%, respectively). Such tails were also found, although to a lesser extent, in sequences from control cells or *rio2* siRNA-treated cells (22 and 20%, respectively). In contrast, only 4% of sequences had U tails in pre-RNA from siRNA *rps15*-treated cells (Supplementary Figure S4). Correlation of poly-uridine tail enrichment with accumulation of 18S-E pre-rRNA in the cytoplasm was confirmed by 3′-RACE on RNAs from cell fractionation: 23% of cytoplasmic sequences presented U tails, whereas only 7% of nuclear sequences had a U tail (data not shown).

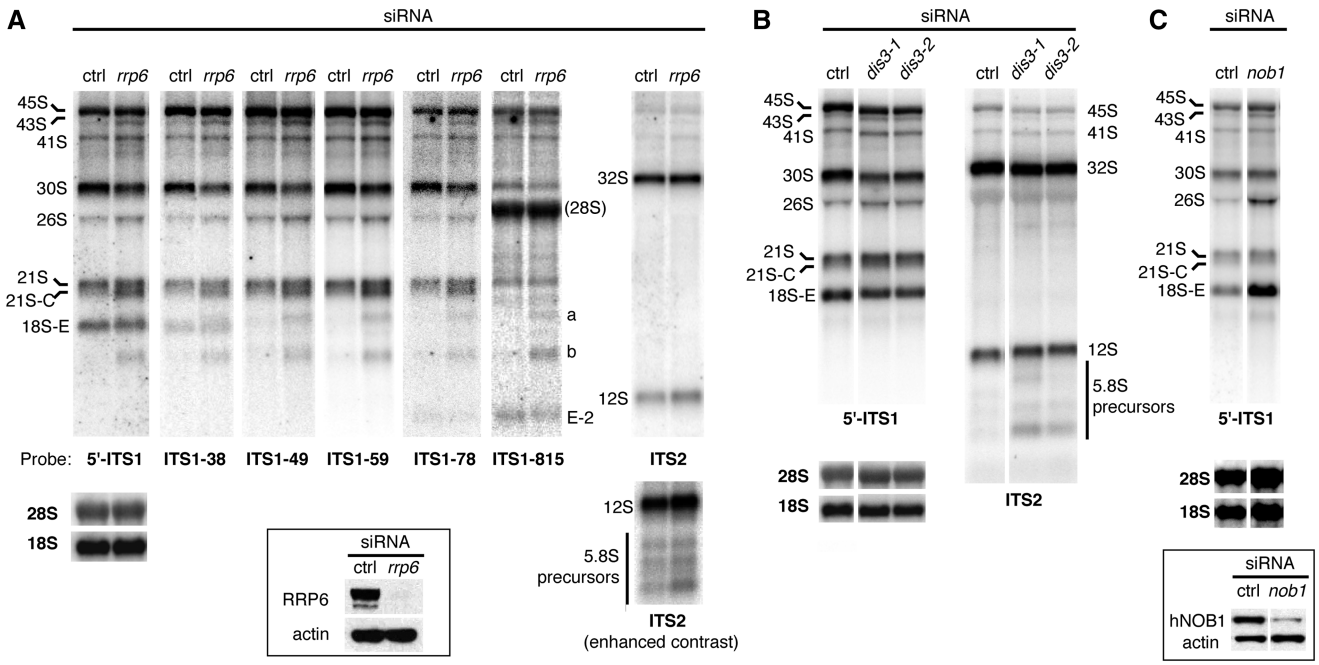

Figure 7. Role of the exosome in human ITS1 processing. RNAs extracted from HeLa cells treated with siRNAs directed against the exosome subunits DIS3 and RRP6, or the putative endonuclease hNOB1, were analyzed by northern blot with various probes complementary to the ITS1 or the ITS2 (Figures 2A and 3C). (**A**) Knocking down RRP6 led to accumulation of the 21S-C pre-rRNA. The 12S pre-rRNA also accumulated together with other precursors to the 5.8S rRNA. The efficiency of RRP6 depletion was assessed by western blot (inset). (**B**) Depletion of DIS3 with two different siRNAs mainly affected maturation of the 5.8S rRNA, as shown with the ITS2 probe. (**C**) Knockdown of hNOB1 prevented maturation of 18S-E pre-rRNA to 18S rRNA. The efficiency of hNOB1 depletion was assessed by western blot (inset).

When 3′-RACE experiments were performed to study the 3′-end of the 21S pre-rRNA in cells treated with siRNAs *rps10* or *rps20* or in control cells, no U tails were found (data not shown), allowing us to exclude that poly-U stretches were artefacts because of the experimental procedure. Poly-uridine synthase activities were previously co-purified with pre-ribosomes (36–39). These results support a role for poly-uridylation in the maturation or the degradation of the 18S-E pre-rRNAs in the cytoplasm.

DISCUSSION

In human cells, formation of the 18S rRNA is currently being envisioned as the result of the endonucleolytic cleavage at site 3 of the 18S-E precursor, which is formed after endonucleolytic cleavage of the ITS1 at site E. The data presented here show that conversion of the 18S-E precursor to mature 18S rRNA is in fact a multi-step process involving 3′–5′ exonucleolytic processing (Figure 8A).

Endonucleolytic cleavage at site E occurs at nucleotide C5605 and C5608

Our results indicate that cleavage E takes place after nucleotides C5605 (+78) and C5608 (+81). Interestingly, both cytidines are followed by a guanosine, suggesting a cleavage at CG dinucleotides. The E-2 fragment is readily detected when stabilized in XRN2-depleted cells, which attests that the 21S pre-rRNA undergoes endonucleolytic cleavage at site E. This cleavage site shares some similarity with the A_2 cleavage site in yeast: both are coupled to elimination of the 5′-ETS, sensitive to depletion of RPS19 or ENP1, and dispensable for maturation of the large subunit. The Rcl1p protein has been proposed to be the site A_2 endonuclease in yeast, which designates the human homolog of Rcl1p as a good candidate to catalyze cleavage at site E (41). However, the sequence of site E does not recapitulate the consensus sequence proposed for Rcl1p. In mouse cells, a cleavage site was detected around position +55 in the ITS1, which is a GU-rich region that has no direct homology with the cleavage site determined here for human cells (42). A nucleolar endoribonuclease able to process the ITS1 around the same position *in vitro* was later purified (43), but the primary target of this endonuclease seemed to be the 18S/ITS1 junction.

The presence in the nucleolus of RNAs with 3′-ends extending downstream of C5608 may indicate the occurrence of additional cleavages. Alternatively, in line with our previous findings (14), we do not exclude that some

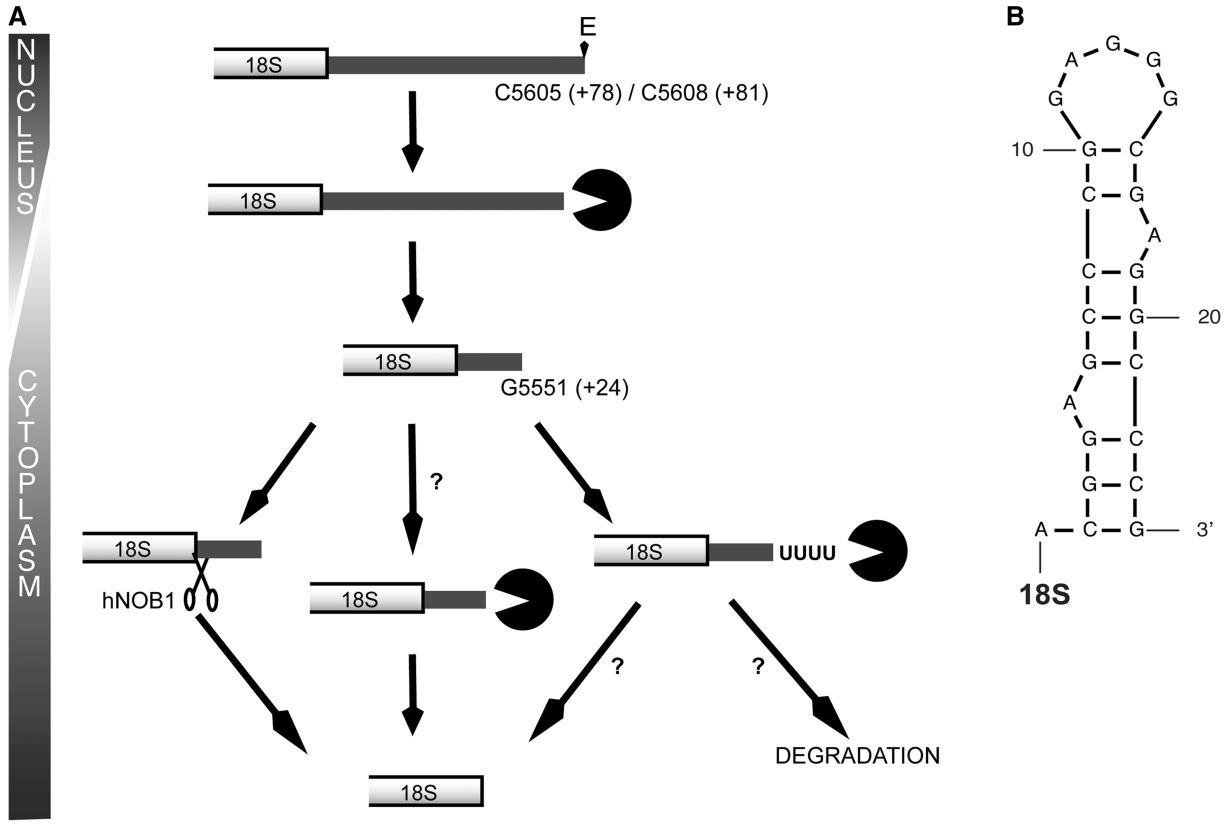

Figure 8. A model for processing of the 18S-E pre-rRNA in human cells. (**A**) The 18S-E pre-rRNA is generated by endonucleolytic cleavage of larger precursors at site E (C5605 or C5608). It is then subjected to 3′–5′ exonucleolytic digestion up to nucleotide G5551 (position +24 of the ITS1). The last nucleotides are likely removed by endonucleolytic cleavage by hNOB1 (like in yeast), but exonucleolytic trimming at this step could represent an alternative pathway. Poly-uridylation observed for the 18S-E/24 intermediate may be part of the maturation pathway or target degradation of stalled precursors. (**B**) A structure prediction of the first 24 nt of the human ITS1 with the Mfold software (40) shows that it can form a stable hairpin.

18S-E pre-rRNA is generated by 3′–5′ exonucleolytic processing of the 21S pre-rRNA. Indeed, knockdown of RRP6 leads to accumulation of the 21S-C intermediate and decreased levels of 18S-E pre-rRNA. This suggests that the exosome may ensure processing of the 21S-C pre-rRNA to 18S-E pre-rRNA. Formation of the 18S-E pre-rRNA could thus be produced from the 21S pre-rRNA through different pathways. Alternatively, the longer species of the 18S-E pre-rRNA detected in the nucleolus may correspond to pre-rRNA degradation products through quality control mechanisms.

Endonucleolytic cleavage at site E is followed by 5′–3′ exonucleolytic processing

Our results indicate that cleavage at site E is followed by exonucleolytic cleavage in both directions. Here, we show that, as described before in mouse (24), the human 36S pre-rRNA is processed by the 5′–3′ exonuclease XRN2. This processing step may yield functional 32S pre-rRNA, as previously shown in mouse (44). However, while it is a major precursor in rodent cells (24), the 36S pre-rRNA is rare in human cells (14), indicating that direct cleavage at site E of the 45S or 41S precursors represents a minor processing pathway. Alternatively, XRN2 may be more active in human cells than in murine cells. XRN2 is also involved in degradation of the ITS1 fragment generated by cleavage at site E of the 21S pre-rRNA.

A highly conserved region in the ITS1 regulating the progression of exonucleases?

After RPL26 or PES1 knockdown, we observed accumulation of a species migrating between the 36S and the 32S pre-rRNAs, which we named 36S-C. This species likely results from an arrest of XRN2 processing rather than from endonucleolytic cleavage, as no complementary fragment was detected. Strikingly, the 5′-end of this intermediate corresponds to the 5′-boundary of the most conserved stretch in ITS1 among mammals (Supplementary Figure S2); likewise, the 3′-end of this region corresponds to the 3′-extremity of the 21S-C pre-rRNA, which results from 3′ to 5′ exonucleolytic trimming of the 21S pre-rRNA and accumulates after knockdown of ENP1 (14), RPS19 (19) or RRP6 (this work). We hypothesize that this segment might be a nodal point for the control of ITS1 processing. Strong secondary structures and/or the binding of specific maturation factors could prevent progression of the exonucleases. Several short stretches in this domain are complementary to the mature rRNAs, which also open the possibility that this region hybridizes with these segments in pre-rRNAs and serves as a folding chaperone.

Formation of the 18S rRNA 3′-end requires 3′–5′ exonucleolytic processing

Unexpectedly, the 3′-RACE experiments showed that endonucleolytic cleavage at site E is also followed by 3′–5′ exonucleolytic processing of the 18S-E pre-rRNA. The higher frequency of fragments ending around positions +35–40 and +24 in total RNAs, confirmed by RNase protection assays, may correspond to pausing of the exonuclease because of secondary structures, as shown for the first 24 nt of the ITS1, which can form a hairpin structure (Figure 8B).

This exonucleolytic maturation is coupled with nuclear export and may be envisioned as a biphasic process (Figure 8A). Processing of the 18S-E pre-rRNA starts right after endonucleolytic cleavage in the nucleolus, as shown by the abundance of RNAs ending between nucleotide +40 and +78 in the nucleolar fraction. Nuclear retention of the pre-40S particles by knockdown of RPS15 did not prevent formation of the 18S-E/24 form, which indicates that the exonuclease is already present in the nucleus. However, this form was more abundant in the cytoplasm than in the nucleus, suggesting that it is mainly formed after nuclear export, or that it is rapidly exported after being generated. Interestingly, it was previously shown that processing of the 3′-end of the 18S rRNA was preserved in a mini-gene containing 103 nt in the ITS1, but it was abolished when only 45 nt were left (45). In light of our data, this result suggests that this first phase of the 18S-E pre-rRNA maturation is required for formation of the 3′-end of the 18S rRNA.

The second phase corresponds to elimination of the last 24 nt in the cytoplasm, which is specifically blocked by knockdown of RPS10, RPS20 or RIO2. In the yeast *S. cerevisiae*, formation of the 18S rRNA 3′-end is ensured by the endonuclease Nob1p (35), whose human homolog hNOB1 was found in pre-40S particles extracted from HeLa cells (27). Accordingly, we show here that knockdown of hNOB1 results in deficient processing of the 18S-E pre-rRNA, which strongly supports that hNOB1 has a similar function as its yeast ortholog. But the presence of 3′-extremities shorter than 24 nt in total or cytoplasmic RNAs (Figures 4A and 5A) suggests that formation of the 18S rRNA 3′-end may be ensured by exonucleolytic processing, similar to the 5.8S rRNA. Consistent with this hypothesis, RNAs ending before position +24 were poorly detected in the nuclear and nucleolar fractions (Figure 5A) or after depletion of RPS10, RPS20 or RIO2 (Figure 6A). Thus, generation of these RNAs occurs in the cytoplasm and is controlled by proper assembly of the pre-40S subunit; their detection in the 3′-RACE experiments is not a mere experimental artefact. If these RNAs were degradation products, one would expect their presence under conditions where pre-40S particle maturation is blocked in the cytoplasm, which is not the case.

A number of exonucleases are candidates for 3′–5′ processing of the 18S-E pre-rRNA after cleavage at site E, starting with the exosome subunits DIS3 and RRP6. Our results do not support an exclusive role of the exosome in 18S-E pre-rRNA processing, as we see no clear contribution of DIS3 and RRP6 under conditions where their knockdown does affect 5.8S rRNA maturation. However, the strong effect of RRP6 depletion on the maturation of the 21S pre-rRNA may hamper the observation of RRP6 activity in 18S-E pre-rRNA trimming, and more work is required to identify the exonucleases involved in this process.

Poly-uridylation of the 18S-E pre-rRNA in the cytoplasm: a tag for maturation or for degradation?

We show here the presence of small poly-U tails at the 3′-end of cytoplasmic 18S-E pre-rRNA, the 18S-E/24 form being the most frequently poly-uridylated species (Supplementary Figure S4). Noticeably, a poly-U polymerase activity was already found associated with eukaryotic ribosomes (36–39). Poly-U polymerases with different functions have been described in several organisms [see (46) and (47) for review]. In human, a nucleolar poly-U polymerase is implicated in the recycling of U6 snRNA after splicing (48,49), whereas two cytoplasmic poly-U polymerases are involved in histone mRNA degradation (50). Similarly, the poly-U tails observed on the 18S-E RNA might act as a signal for cytoplasmic nucleases to engage the final maturation of the 24-nt form. Alternatively, it might target the 18S-E pre-rRNAs for degradation by the exosome similar to the short poly-A tails added on nuclear pre-rRNAs, which is mediated in yeast by the Trf4/Air2/Mtr4 Polyadenylation complex (TRAMP) complex (29) and was recently shown to involve the poly(A) polymerase-associated domain-containing protein 5 in murine cells (51). In this respect, the higher proportion of poly-uridylated 18S-E pre-rRNA after depletion of RPS10, RPS20 or RIO2 may reflect a more intense degradation activity because of stalled processing, or accumulation of the poly-uridylated particles unable to recruit the final maturation enzyme.

CONCLUSION

These data deliver a new and complex picture of ITS1 processing in mammalian cells, which combines the activity of endonucleases with that of 5′–3′ and 3′–5′ exonucleases. Exonucleases, which also participate in RNA degradation, can couple RNA processing and quality control. Evolution of ribosome biogenesis mechanisms in mammals may have led to increased levels of control compared with yeast and to redundant mechanisms for 18S rRNA formation. Importantly, these results define a mechanistic framework to study the interplay of several DBA-linked ribosomal proteins that are known to be required at various steps of ITS1 processing: RPL26 in cleavage at site 2 and exonucleolytic degradation of the ITS1; RPS19 and RPS17 in cleavage at site E; RPS10 and RPS26 in the final maturation steps of the 18S rRNA. It remains to determine which enzymes are involved in these mammalian-specific maturation mechanisms, and whether these observations can be extended to other metazoans.

SUPPLEMENTARY DATA

Supplementary Data are available at NAR Online: Supplementary Figures 1–4 and Supplementary Reference [52].

ACKNOWLEDGEMENTS

The authors are grateful to Dr Michèle Caizergues-Ferrer, Dr Marlène Faubladier, Dr Jérôme Cavaillé, Dr Anthony Henras, Dr Yves Henry, Dr Tamas Kiss, Dr Hervé Seitz and their colleagues at LBME for fruitful discussions, technical advice and reagents.

FUNDING

CNRS; University of Toulouse; French National Research Agency (ANR—RIBOCRASH project); Institut Universitaire de France. Funding for open access charge: ANR.

Conflict of interest statement. None declared.

REFERENCES

1. Fumagalli,S. and Thomas,G. (2011) The role of p53 in ribosomopathies. *Semin. Hematol.*, **48**, 97–105.
2. Donati,G., Montanaro,L. and Derenzini,M. (2012) Ribosome biogenesis and control of cell proliferation: p53 is not alone. *Cancer Res.*, **72**, 1602–1607.
3. Chakraborty,A., Uechi,T. and Kenmochi,N. (2011) Guarding the 'translation apparatus': defective ribosome biogenesis and the p53 signaling pathway. *WIRE RNA*, **2**, 507–522.
4. Ellis,S.R. and Gleizes,P.-E. (2011) Diamond Blackfan anemia: ribosomal proteins going rogue. *Semin. Hematol.*, **48**, 89–96.
5. Boria,I., Garelli,E., Gazda,H.T., Aspesi,A., Quarello,P., Pavesi,E., Ferrante,D., Meerpohl,J.J., Kartal,M., Da Costa,L. *et al.* (2010) The ribosomal basis of Diamond-Blackfan Anemia: mutation and database update. *Hum. Mutat.*, **31**, 1269–1279.
6. Dutt,S., Narla,A., Lin,K., Mullally,A., Abayasekara,N., Megerdichian,C., Wilson,F.H., Currie,T., Khanna-Gupta,A., Berliner,N. *et al.* (2011) Haploinsufficiency for ribosomal protein genes causes selective activation of p53 in human erythroid progenitor cells. *Blood*, **117**, 2567–2576.
7. Narla,A. and Ebert,B.L. (2010) Ribosomopathies: human disorders of ribosome dysfunction. *Blood*, **115**, 3196–3205.
8. Burwick,N., Shimamura,A. and Liu,J.M. (2011) Non-Diamond Blackfan anemia disorders of ribosome function: Shwachman Diamond syndrome and 5q-syndrome. *Semin. Hematol.*, **48**, 136–143.
9. Fatica,A. and Tollervey,D. (2002) Making ribosomes. *Curr. Opin. Cell Biol.*, **14**, 313–318.
10. Fromont-Racine,M., Senger,B., Saveanu,C. and Fasiolo,F. (2003) Ribosome assembly in eukaryotes. *Gene*, **313**, 17–42.
11. Henras,A.K., Soudet,J., Gérus,M., Lebaron,S., Caizergues-Ferrer,M., Mougin,A. and Henry,Y. (2008) The post-transcriptional steps of eukaryotic ribosome biogenesis. *Cell. Mol. Life Sci.*, **65**, 2334–2359.
12. Granneman,S. and Baserga,S.J. (2004) Ribosome biogenesis: of knobs and RNA processing. *Exp. Cell Res.*, **296**, 43–50.
13. Rouquette,J., Choesmel,V. and Gleizes,P.-E. (2005) Nuclear export and cytoplasmic processing of precursors to the 40S ribosomal subunits in mammalian cells. *EMBO J.*, **24**, 2862–2872.
14. Carron,C., O'Donohue,M.-F., Choesmel,V., Faubladier,M. and Gleizes,P.-E. (2011) Analysis of two human pre-ribosomal factors, bystin and hTsr1, highlights differences in evolution of ribosome biogenesis between yeast and mammals. *Nucleic Acids Res.*, **39**, 280–291.
15. Hadjiolova,K.V., Nicoloso,M., Mazan,S., Hadjiolov,A.A. and Bachellerie,J.P. (1993) Alternative pre-rRNA processing pathways in human cells and their alteration by cycloheximide inhibition of protein synthesis. *Eur. J. Biochem.*, **212**, 211–215.
16. Gerbi,S.A. and Borovjagin,A.V. (2004) Pre-ribosomal RNA processing in multicellular organisms. In: Olson,M.O.J. (ed.), *The Nucleolus*. Eurekah.com and Kluwer Academic/Plenum Publishers, New York, pp. 170–198.
17. Choesmel,V., Bacqueville,D., Rouquette,J., Noaillac-Depeyre,J., Fribourg,S., Crétien,A., Leblanc,T., Tchernia,G., Da Costa,L. and Gleizes,P.-E. (2007) Impaired ribosome biogenesis in Diamond-Blackfan anemia. *Blood*, **109**, 1275–1283.

18. Flygare,J., Aspesi,A., Bailey,J.C., Miyake,K., Caffrey,J.M., Karlsson,S. and Ellis,S.R. (2007) Human RPS19, the gene mutated in Diamond-Blackfan anemia, encodes a ribosomal protein required for the maturation of 40S ribosomal subunits. *Blood*, **109**, 980–986.
19. Idol,R.A., Robledo,S., Du,H.-Y., Crimmins,D.L., Wilson,D.B., Ladenson,J.H., Bessler,M. and Mason,P.J. (2007) Cells depleted for RPS19, a protein associated with Diamond Blackfan Anemia, show defects in 18S ribosomal RNA synthesis and small ribosomal subunit production. *Blood Cells Mol. Dis.*, **39**, 35–43.
20. Doherty,L., Sheen,M.R., Vlachos,A., Choesmel,V., O'Donohue,M.-F., Clinton,C., Schneider,H.E., Sieff,C.A., Newburger,P.E., Ball,S.E. *et al.* (2010) Ribosomal protein genes RPS10 and RPS26 are commonly mutated in Diamond-Blackfan anemia. *Am. J. Hum. Genet.*, **86**, 222–228.
21. Cmejla,R., Cmejlova,J., Handrkova,H., Petrak,J. and Pospisilova,D. (2007) Ribosomal protein S17 gene (RPS17) is mutated in Diamond-Blackfan anemia. *Hum. Mutat.*, **28**, 1178–1182.
22. Gazda,H.T., Preti,M., Sheen,M.R., O'Donohue,M.-F., Vlachos,A., Davies,S.M., Kattamis,A., Doherty,L., Landowski,M., Buros,C. *et al.* (2012) Frameshift mutation in p53 regulator RPL26 is associated with multiple physical abnormalities and a specific pre-rRNA processing defect in Diamond-Blackfan anemia. *Hum. Mutat.*, **33**, 1037–1044.
23. Kiss,T. and Filipowicz,W. (1993) Small nucleolar RNAs encoded by introns of the human cell cycle regulatory gene RCC1. *EMBO J.*, **12**, 2913–2920.
24. Wang,M. and Pestov,D.G. (2011) 5′-end surveillance by Xrn2 acts as a shared mechanism for mammalian pre-rRNA maturation and decay. *Nucleic Acids Res.*, **39**, 1811–1822.
25. O'Donohue,M.-F., Choesmel,V., Faubladier,M., Fichant,G. and Gleizes,P.-E. (2010) Functional dichotomy of ribosomal proteins during the synthesis of mammalian 40S ribosomal subunits. *J. Cell Biol.*, **190**, 853–866.
26. Sahasranaman,A., Dembowski,J., Strahler,J., Andrews,P., Maddock,J. and Woolford,J.L. (2011) Assembly of Saccharomyces cerevisiae 60S ribosomal subunits: role of factors required for 27S pre-rRNA processing. *EMBO J.*, **30**, 4020–4032.
27. Zemp,I., Wild,T., O'Donohue,M.-F., Wandrey,F., Widmann,B., Gleizes,P.-E. and Kutay,U. (2009) Distinct cytoplasmic maturation steps of 40S ribosomal subunit precursors require hRio2. *J. Cell Biol.*, **185**, 1167–1180.
28. Mitchell,P., Petfalski,E., Shevchenko,A., Mann,M. and Tollervey,D. (1997) The exosome: a conserved eukaryotic RNA processing complex containing multiple 3′–>5′ exoribonucleases. *Cell*, **91**, 457–466.
29. LaCava,J., Houseley,J., Saveanu,C., Petfalski,E., Thompson,E., Jacquier,A. and Tollervey,D. (2005) RNA degradation by the exosome is promoted by a nuclear polyadenylation complex. *Cell*, **121**, 713–724.
30. Briggs,M.W., Burkard,K.T. and Butler,J.S. (1998) Rrp6p, the yeast homologue of the human PM-Scl 100-kDa autoantigen, is essential for efficient 5.8 S rRNA 3′ end formation. *J. Biol. Chem.*, **273**, 13255–13263.
31. Dziembowski,A., Lorentzen,E., Conti,E. and Séraphin,B. (2007) A single subunit, Dis3, is essentially responsible for yeast exosome core activity. *Nat. Struct. Mol. Biol.*, **14**, 15–22.
32. Staals,R., Bronkhorst,A., Schilders,G., Slomovic,S., Schuster,G., Heck,A., Raijmakers,R. and Pruijn,G. (2010) Dis3-like 1: a novel exoribonuclease associated with the human exosome. *EMBO J.*, **29**, 2358–2367.
33. Tomecki,R., Kristiansen,M., Lykke-Andersen,S., Chlebowski,A., Larsen,K., Szczesny,R., Drazkowska,K., Pastula,A., Andersen,J.S., Stepien,P. *et al.* (2010) The human core exosome interacts with differentially localized processive RNases: hDIS3 and hDIS3L. *EMBO J.*, **29**, 2342–2357.
34. Astuti,D., Morris,M., Cooper,W., Staals,R., Wake,N., Fews,G., Gill,H., Gentle,D., Shuib,S., Ricketts,C. *et al.* (2012) Germline mutations in DIS3L2 cause the Perlman syndrome of overgrowth and Wilms tumor susceptibility. *Nat. Genet.*, **44**, 277–284.
35. Pertschy,B., Schneider,C., Gnadig,M., Schafer,T., Tollervey,D. and Hurt,E. (2009) RNA helicase Prp43 and its co-factor Pfa1 promote 20 to 18 S rRNA processing catalyzed by the endonuclease Nob1. *J. Biol. Chem.*, **284**, 35079–35091.
36. Wilkie,N.M. and Smellie,R.M. (1968) Polyribonucleotide synthesis by subfractions of microsomes from rat liver. *Biochem. J.*, **109**, 229–238.
37. Hozumi,N., Haruna,I., Watanabe,I., Mikoshiba,K. and Tsukada,Y. (1975) Poly(U) polymerase in rat brain. *Nature*, **256**, 337–339.
38. Milchev,G.I. and Hadjiolov,A.A. (1978) Association of poly(A) and poly(U) polymerases with cytoplasmic ribosomes. *Eur. J. Biochem.*, **84**, 113–121.
39. Hayashi,T.T. and MacFarlane,K. (1979) Comparison of endogenous and exogenous RNA primers of poly(U) polymerase in rat hepatic ribosomes. *Biochem. J.*, **177**, 895–902.
40. Zuker,M. (2003) Mfold web server for nucleic acid folding and hybridization prediction. *Nucleic Acids Res.*, **31**, 3406–3415.
41. Horn,D.M., Mason,S.L. and Karbstein,K. (2011) Rcl1 protein, a novel nuclease for 18 S ribosomal RNA production. *J. Biol. Chem.*, **286**, 34082–34087.
42. Raziuddin, Little,R.D., Labella,T. and Schlessinger,D. (1989) Transcription and processing of RNA from mouse ribosomal DNA transfected into hamster cells. *Mol. Cell. Biol.*, **9**, 1667–1671.
43. Shumard,C.M., Torres,C. and Eichler,D.C. (1990) In vitro processing at the 3′-terminal region of pre-18S rRNA by a nucleolar endoribonuclease. *Mol. Cell. Biol.*, **10**, 3868–3872.
44. Strezoska,Z., Pestov,D.G. and Lau,L.F. (2000) Bop1 is a mouse WD40 repeat nucleolar protein involved in 28S and 5. 8S rRNA processing and 60S ribosome biogenesis. *Mol. Cell. Biol.*, **20**, 5516–5528.
45. Cavaillé,J., Hadjiolov,A.A. and Bachellerie,J.P. (1996) Processing of mammalian rRNA precursors at the 3′ end of 18S rRNA. Identification of cis-acting signals suggests the involvement of U13 small nucleolar RNA. *Eur. J. Biochem.*, **242**, 206–213.
46. Rissland,O.S. and Norbury,C.J. (2008) The Cid1 poly(U) polymerase. *Biochim. Biophys. Acta*, **1779**, 286–294.
47. Wilusz,C.J. and Wilusz,J. (2008) New ways to meet your (3′) end oligouridylation as a step on the path to destruction. *Genes Dev.*, **22**, 1–7.
48. Trippe,R., Richly,H. and Benecke,B.-J. (2003) Biochemical characterization of a U6 small nuclear RNA-specific terminal uridylyltransferase. *Eur. J. Biochem.*, **270**, 971–980.
49. Trippe,R., Guschina,E., Hossbach,M., Urlaub,H., Lührmann,R. and Benecke,B.-J. (2006) Identification, cloning, and functional analysis of the human U6 snRNA-specific terminal uridylyl transferase. *RNA*, **12**, 1494–1504.
50. Mullen,T.E. and Marzluff,W.F. (2008) Degradation of histone mRNA requires oligouridylation followed by decapping and simultaneous degradation of the mRNA both 5′ to 3′ and 3′ to 5′. *Genes Dev.*, **22**, 50–65.
51. Shcherbik,N., Wang,M., Lapik,Y.R., Srivastava,L. and Pestov,D.G. (2010) Polyadenylation and degradation of incomplete RNA polymerase I transcripts in mammalian cells. *EMBO Rep.*, **11**, 106–111.
52. Waterhouse,A.M., Procter,J.B., Martin,D.M.A., Clamp,M. and Barton,G.J. (2009) Jalview Version 2–a multiple sequence alignment editor and analysis workbench. *Bioinformatics*, **25**, 1189–1191.